Chemical Engineering Science 167 (2017) 66–77

Contents lists available at ScienceDirect

Chemical Engineering Science

journal homepage: www.elsevier.com/locate/ces

Modeling and optimization of spherical agglomeration in suspension through a coupled population balance model

Ramon Peña [a], Christopher L. Burcham [b], Daniel J. Jarmer [b], Doraiswami Ramkrishna [a], Zoltan K. Nagy [a,*]

[a] School of Chemical Engineering, Purdue University, West Lafayette, IN 47907, United States
[b] Eli Lilly and Company, Indianapolis, IN 46285, United States

HIGHLIGHTS

- A coupled population balance model for spherical agglomeration systems is proposed.
- The model enables simulation of crystals and agglomerate particles independently.
- First principles based process parameters (i.e. agglomeration efficiency, porosity).
- Optimization framework for both bioavailability and manufacturability targeting.
- The proposed model can lead to improved parameter estimation and kinetic studies.

ARTICLE INFO

Article history:
Received 8 November 2016
Received in revised form 24 February 2017
Accepted 28 March 2017
Available online 31 March 2017

Keywords:
Population balance model
Spherical crystallization
Agglomeration in suspension

ABSTRACT

The population balance model is the common approach to simulation and prediction of the size distribution and other properties of particulate systems. Population balance models include any nucleation, growth, breakage and agglomeration mechanisms that are relevant to all industrial particulate processes. However, there are some limitations to many of the previous population balance model formulations for systems with agglomeration. Limitations include physically irrelevant and/or empirically based agglomeration kernels, difficulties in assessing the influence of process conditions (e.g. hydrodynamics, particulate physical properties), solution method efficiency for optimization and control applications, and loss of information on constituent particles. These limitations have prevented the use of population balance models to accurately predict and simulate agglomeration in suspension techniques such as spherical crystallization. To overcome these limitations, an extension of the concept of a coupled population balance model is presented for application in the simulation and optimization of a spherical crystallization system. A coupled population balance model formulation has been developed for a semi-batch, reverse addition, anti-solvent crystallization system with agglomeration. The system includes nucleation and growth of the primary crystals and subsequent agglomeration. The advantages presented by a coupled population balance model formulation include the ability to optimize for specific primary and agglomerate sizes. This presents an opportunity to find optimal operating conditions that meet both bioavailability and manufacturability demands.

1. Introduction

Since its introduction, the population balance model (PBM) has been widely used and accepted as the model formulation method for simulation and prediction of the size distribution and other properties of particulate systems (Randolph and Larson, 1971; Ramkrishna, 2000). PBMs allow for systems that include any or all of the following mechanisms: nucleation, growth, breakage and agglomeration. Following the initial work by Smoluchowski (Smoluchowski, 1917) on the rate of aggregation for spherical particles, there have been many contributions for systems that exhibit agglomeration including dispersion (bubble) coalescence (Coulaloglou and Tavlarides, 1977; Prince and Blanch, 1990), granulation (Iveson, 2002; Liu and Litster, 2002) and particle aggregation during crystallization (Marchal et al., 1988; David et al., 1990; Kumar and Ramkrishna, 1997). The shared limitation in the models between many of the previous studies is the loss of information of constituent particles. This limitation presents obstacles in the estimation of the kinetic parameters (nucleation and

* Corresponding author.
E-mail address: zknagy@purdue.edu (Z.K. Nagy).

http://dx.doi.org/10.1016/j.ces.2017.03.055
0009-2509/

Nomenclature

$n_{tc}(x,t)$	number density (no. m^{-4}) representing the primary crystals
$n_{cs}(x,t)$	number density (no. m^{-4}) representing the un-agglomerated crystals
$n_a(x,t)$	number density (no. m^{-4}) representing the agglomerates
$n_{ca}(\lambda,t)$	number density (no. m^{-4}) representing the un-agglomerated crystals and agglomerates
G	growth rate (m s^{-1})
B	nucleation rate (no. m^{-3} s^{-1})
$\delta(x)$	dirac delta function (m^{-1})
$\beta(x,\lambda)$	agglomeration rate (m^3 no. $^{-1}$ s^{-1})
$D_{cs,agg}(x)$	death (disappearance) of crystals in suspension due to agglomeration (no. m^{-1} s^{-1})
$B_{a,agg}(x)$	birth of agglomerates from crystal and agglomerate interactions (no. m^{-1} s^{-1})
$D_{a,agg}(x)$	death of agglomerates from crystal and agglomerate interactions (no. m^{-1} s^{-1})
$V(t)$	suspension volume (m^3)
x, λ	characteristic length (m)
t	batch time
$\tilde{n}(x,t) = V(t)n(x,t)$	redefined (non-volumetric) number density
w_i	weights
L_i	abscissas
F_s	solution flow rate (mL/min)
C_S	solute (benzoic acid) concentration (g mL^{-1})
C_{in}	solution concentration (g mL^{-1})
x_{SASR}	solution to anti-solvent ratio
ρ_c	crystal density
k_v	shape factor
S	supersaturation
$\mathcal{SASR}$	solution to anti-solvent ratio
$\mathcal{N}$	agitation rate
k_g, g, k_b, b	growth and nucleation rate constants
ε	energy dissipation (W kg^{-1})
N_p	stirrer power number
d_s	diameter of the stirrer (m)
$\mathcal{AE}$	agglomeration efficiency
$\mathcal{P}$	porosity
$\mathcal{C}_{final}$	final concentration of solute (g mL^{-1})
C_{max}	maximum concentration
$\beth_i$	optimization weights
$\mathcal{B}_T$	bioavailability target
$\mathcal{M}_T$	manufacturability target
$\mathcal{L}_{tc,10}$, $\mathcal{L}_{a,10}$	first moment based mean size
$\mathcal{V}_{tc,30}, \mathcal{V}_{cs,30}, \mathcal{V}_{a,30}$	third moment based mean volume

growth rate vs agglomeration rate) and in developing an understanding of the influence of process conditions on each in population (constituent particles vs agglomerates). Having information regarding the constituent particles would allow for improved particle design through more accurate parameter estimation, simulation, optimization, and control; particularly for the increasingly popular technique of agglomeration in suspension.

Agglomerating fine particles in suspension, through the use of a bridging liquid, to improve particle properties and downstream process efficiency has been known since the late 1960s. Initially, the technique was used mostly in bulk chemical industries, e.g. coal beneficiation (Petela, 1991). Since then agglomeration in suspension techniques have been geared towards application in the pharmaceutical industry to improve filtration and downstream processing of active pharmaceutical ingredient (API) during crystallization by eliminating granulation and milling unit operations (Kawashima, 1984; Kawashima et al., 2003; Amaro-González and Biscans, 2002). In this respect the technique is often referred to as spherical crystallization. Interest in the application of spherical crystallization in pharmaceutical processes has increased through the continued development and understanding of the operating conditions (Kawashima et al., 1982a, 1982b; Kawashima, 1995), choice of binding agent (Katta and Rasmuson, 2008), kinetics (Kawashima and Capes, 1974) and mechanisms (Kawashima et al., 2003; Rasmuson and Thati, 2011; Thati and Rasmuson, 2012; Blandin et al., 2003) that govern experimental outcomes. Peña and Nagy (2015) studied and showed the benefits of spherical crystallization as a process intensification technique, whereby both internal (primary crystals) and external (agglomerates) properties can be controlled experimentally through a decoupled continuous spherical crystallization (CSC) approach; providing the means by which both biopharmaceutical (bioavailability, dissolution) and manufacturing (flowability, filtration, drying) properties can be simultaneously adapted to meet desired quality specifications. This technique opens the door for combined experimental and modeling approaches for the optimization and control of both the primary crystal and agglomerate properties in spherical crystallization processes. However, many of the PBMs currently in literature would fail to accomplish this because of the aforementioned limitations and loss of constituent particle information.

The limitations in previously developed PBMs are related to the complex crystallization phenomena occurring during spherical crystallization processes. For previous models, agglomeration was either an incidental process occurring along with nucleation and growth during crystallization or the main process occurring in seeded or seed-fed systems with negligible nucleation and growth. This allowed for empirical agglomeration models often independent of system properties and solely dependent on fitting to experimental data (Seyssiecq et al., 2000). The accuracy of those models are limited, are very system dependent and have difficulty capturing all the influencing process parameters on the system. Moreover, they only take into consideration the evolution of the agglomerates and not that of the constituent primary crystals. As previously mentioned, from the mechanistic point of view there are numerous studies in the literature that propose agglomeration mechanisms. However, there has yet to be a comprehensive correlation between the proposed mechanisms of spherical crystallization, which include nucleation, growth and agglomeration, and the appropriate agglomeration kernel. This has largely been influenced by the inherit loss of information in the PBMs and the lack of process analytical technology (PAT) tools to help determine and validate proposed mechanisms (Nagy et al., 2013).

Bemer (1979) was one of the first to study agglomeration in suspension from both an experimental and modeling approach. His work led to further implementations of combined experimental and modeling studies. David et al. (2003) developed a multilayer agglomeration model that considers the efficiency of agglomeration based on the collision mechanism (i.e. Brownian, laminar, or turbulent). As particles change in size their collision mechanism or flow field can change from Brownian to laminar to turbulent, as particle size increases. In their model, the kernel accounted for changes in the collision mechanism and was also a function of the supersaturation and temperature through the growth rate which was used as the efficiency term. It is known that

agglomeration is enhanced by inter-particle growth or agglomerative bond formation; when supersaturation increases the subsequent inter-particle growth between two particles that come in contact increases allowing for higher agglomeration efficiency (Brunsteiner et al., 2005). Madec et al. (2003) simplified the agglomeration model by incorporating a more relevant process parameter into the kernel, specifically their work accounted for the composition of bridging liquid in an agglomerate. It has been shown that there is a critically optimal range for the ratio of bridging liquid to solute volume (BSR); below or above this critically optimal range would produce loosely compacted agglomerates or paste-like amorphous agglomerates, respectively (Petela, 1991; Thati and Rasmuson, 2012; Peña and Nagy, 2015). This unique incorporation of the bridging liquid composition served as the efficiency term by which the process would reach equilibrium.

The most comprehensive study in this area is that of Blandin et al. (2005). In this combined experimental and modeling study, key aspects of agglomeration in suspension are noted:

(1) The agglomeration mechanism is a three-step process; (i) bridging liquid droplets capture solid particles and form agglomerate nuclei, (ii) compaction of the agglomerate nuclei due to collisions with other particles causes a rapid decrease in the mean diameter, (iii) growth and consolidation then occur due to the hydrodynamics and process conditions of the system (i.e. collisions, BSR).
(2) Agglomeration is only efficient in the critical BSR range; the agglomerate size increases with a strong dependence on BSR, weak dependence on solids concentration and inverse dependence on agitation rate.
(3) Porosity decreases as mean diameter reaches equilibrium.
(4) Agglomeration stops once the agglomerates become too compact to deform.

Based on these fundamental experimental observations an agglomeration model considering the size and concentration of the agglomerating particles, with the agglomeration kernel expressed as a function of the *meeting probability* and agglomeration efficiency of the process, was developed. The meeting probability was described by a function of the target efficiency, agglomerate sizes, and collision velocity (Kuboi et al., 1984). The simulations from this work were in agreement with experimental data when the necessary parameters were fit to the data. By identifying the critical experimental mechanisms, Blandin et al. was able to develop a comprehensive model that accounted for both the mechanistic phenomena (e.g. deformability, collision efficiency, and compaction) and process conditions (e.g. energy dissipation, BSR, primary particle size). Although this model showed significant superiority over many others observed in the literature, it still has the limitation of losing the information of the constituent particles. Moreover, the model relies on the assumption that the initial particles participating in the agglomeration are monodispersed. Table 1 summarizes various kernels found in the literature used for agglomeration in suspension modeling with r defined as the radius of the particle and is interchangeable with the characteristic length.

To overcome the issues of loss of information a coupled PBM formulation is required. A coupled PBM formulation could simultaneously tracks the evolution of the primary crystals and the evolution of the agglomerates. The relationship between primary crystal properties and their effect on final agglomerate properties would thereby be more evident and more efficient than in traditional approaches. To the best of our knowledge, the only previous work that presented this approach is that of Ochsenbein et al. (2015). In their study, Ochsenbein et al. focused on the agglomeration of needle-like crystals in suspension. Through a coupled PBM framework Ochsenbein et al. were able to develop a population balance equation (PBE) to describe the evolution of the primary crystals by a two-dimensional growth rate to represent the needle like structure of the crystal. Then another PBE was used to describe the evolution of the agglomerates as a function of the primary crystals. For the agglomeration kernel, they derived their own modified kernel that included both characteristic lengths of the primary crystals participating in the agglomeration. The new PBM formulation also allowed for the development of new parameters that add value to the simulations due to their experimental relevance. However, the work of Ochsenbein et al. neglected nucleation, something common to previously developed PBMs with agglomeration. The coupled population balance model framework will be extended herein.

Table 1
Common agglomeration kernels.

Size-independent	K_a
Product	$K_a(r_i r_j)^3$
Sum	$K_a(r_i^3 + r_j^3)$
Brownian (Smoluchowski, 1917)	$K_a \frac{(r_i+r_j)}{(r_i * r_j)}$
Shear	$K_a(r_i + r_j)^3$
Modified Shear	$K_a \alpha_{i,j}(r_i + r_j)^3$
Turbulent	$K_a(r_i + r_j)^2 \sqrt{\overline{U_i^2} + \overline{U_j^2}}$
Zauner and Jones (2000)	$5.431 * 10^{-17}(1 + 2.29\varepsilon^{\frac{1}{2}} - 2.429\varepsilon)S^{2.15}$
Madec et al. (2003)	$K_a(r_i^3 + r_j^3)\left((c_i + c_j)^{\alpha}\left(100 - \frac{c_i+c_j}{2}\right)^{\delta}\right)^{\alpha}$
Blandin et al. (2005) and Kuboi et al. (1984)	$K_a = f(r_i, r_j, t)eff(r_i, r_j, t)$

The contribution of this work is the extension of the coupled PBM framework for application in the simulation and optimization of an agglomeration in suspension system. A coupled PBM framework has been developed for a semi-batch, reverse addition, anti-solvent crystallization system with agglomeration. Reverse addition anti-solvent crystallization techniques entail the addition of solution to the anti-solvent. The technique is carried out for low solution to anti-solvent ratios to produce very fine crystals due to very high supersaturation generation. The system includes nucleation and growth of primary crystals and subsequent agglomeration. The purpose of the work is to exploit the advantages presented by a coupled PBM framework; for example, the ability to optimize for specific primary and agglomerate sizes. This presents an opportunity to find optimal operating conditions that meet both bioavailability and manufacturability demands. It also allows for the ability to develop a first principles based parameter for agglomeration efficiency and a first principles based estimate for porosity. Additionally, through the retention of the information of the primary particles, the interplay between the effects of operating conditions on the properties of the primary crystals versus the agglomerates will be clear.

2. Model development for agglomeration in suspension

Modeling the agglomeration in suspension system is decomposed into three populations: all primary crystals, unagglomerated crystals and agglomerates. The system of coupled population balance equations will be coupled with a mass balance equation to enable the modeling of the crystal size distribution (CSD) properties and agglomerate size distribution (ASD) properties simultaneously. The model will allow us to relate the CSD and ASD properties to micromeritic properties (e.g. porosity and agglomeration efficiency). The PBM will incorporate nucleation, growth and agglomeration mechanisms. This coupling allows for a PBE that describes the entire primary crystal population whether part of an agglomerate or not. However, the PBE does not track the

location of the primary crystals. The inability to track the location of the primary crystals creates a difficulty in assessing the exposure of each individual crystal to supersaturated fluid; especially, once it is incorporated into an agglomerate. Hence, for simplicity, it is assumed that primary crystal growth rate is independent of its in environment (i.e. particles partaking in agglomeration have the same kinetics (growth) as particles remaining in suspension). This assumption is a limitation of the model but studies the literature have shown that agglomerate strength is dependent on supersaturation of the system due to growth of crystals within an agglomerate (agglomerative bond) (Brunsteiner et al., 2005).

The set of PBEs are as follows:

$$\frac{\partial}{\partial t}[V(t)n_{tc}(x,t)] = -\frac{\partial}{\partial x}(G(x)V(t)n_{tc}(x,t)) + \delta(x)V(t)B \tag{1}$$

In Eq. (1), $n_{tc}(x, t)$ is the volumetric number density (no. m^{-4}) representing the primary crystals in the system; regardless of whether the crystal is part of an agglomerate or not (total crystals). G (m s^{-1}) is the growth rate, B (no. m^{-3} s^{-1}) is the nucleation rate, $\delta(x)$ (m^{-1}) is the Dirac delta function, and $V(t)$ (m^3) is the suspension volume. x (m) represents the characteristic length and t is the batch time.

$$\frac{\partial}{\partial t}[V(t)n_{cs}(x,t)] = -\frac{\partial}{\partial x}(G(x)V(t)n_{cs}(x,t)) + \delta(x)V(t)B - D_{cs,agg}(x) \tag{2}$$

$$D_{cs,agg}(x) = V(t)n_{cs}(x,t)\int_0^\infty \beta(x,\lambda)n_{ca}(\lambda,t)d\lambda \tag{3}$$

In Eq. (2), $n_{cs}(x, t)$ is the volumetric number density (no. m^{-4}) representing the un-agglomerated crystals (crystals in suspension). This equation differs from the first equation by the third term ($D_{cs,agg}(x)$ (no. m^{-1} s^{-1})) which represents the death (disappearance) of crystals due to agglomeration (Eq. (3)). The death of crystals can occur through crystal agglomeration with other crystals or agglomerates. This is denoted by the volumetric number density $n_{ca}(\lambda, t)$ (no. m^{-4}) which represents both crystals and agglomerates of a characteristic size λ. In Eq. (3), $\beta(x, \lambda)$ represents the agglomeration rate (m^3 - no.$^{-1}$ s^{-1}) of a particle of characteristic size x with a particle of characteristic size λ.

$$\frac{\partial}{\partial t}[V(t)n_a(x,t)] = -\frac{\partial}{\partial x}(G(x)V(t)n_a(x,t)) + B_{a,agg}(x) - D_{a,agg}(x) \tag{4}$$

$$B_{a,agg}(x) = \frac{x^2}{2}\int_0^x \frac{\beta((x^3-\lambda^3)^{1/3},\lambda)n_{ca}((x^3-\lambda^3),t)V(t)n_{ca}(\lambda,t)}{(x^3-\lambda^3)^{2/3}}d\lambda \tag{5}$$

$$D_{a,agg}(x) = V(t)n_a(x,t)\int_0^\infty \beta(x,\lambda)n_{ca}(\lambda,t)d\lambda \tag{6}$$

In Eq. (4), $n_a(x, t)$ is the volumetric number density (no. m^{-4}) representing the agglomerates produced from the birth ($B_{a,agg}(x)$ (no. m^{-1} s^{-1})) and death ($D_{a,agg}(x)$ (no. m^{-1} s^{-1})) of agglomerates from crystal-agglomerate and agglomerate-agglomerate agglomeration. $\beta(x, \lambda)$ is the same as the term in Eq. (3) and represents the agglomeration rate. It is important to note that traditionally the agglomeration birth and death terms are expressed with volume as the internal coordinate. However, since all the other mechanisms are expressed with respect to characteristic length a modification is made to express this in terms with respect to characteristic length following modification steps from the literature (Marchisio et al., 2003a, 2003b; Costa et al., 2007). Eqs. (2) and (4) are coupled through Eq. (7).

$$n_{ca}(x,t) = n_{cs}(x,t) + n_a(x,t) \tag{7}$$

Eq. (7) is simply the addition of the un-agglomerated crystals and the agglomerates denoted by the number density function $n_{ca}(x, t)$ (no. m^{-4}). This combined population is used to account for crystal-crystal and crystal-agglomerate interactions and reduce the number of terms in the birth and death terms in Eqs. (1)–(6). Eq. (1) is intentionally made to stand alone based on the assumption of uniform kinetics for all populations tracked in the system. The set of equations will all be coupled by the mass balance which will ultimately determine nucleation and growth kinetics.

3. Solution method

Most of the spherical crystallization systems in literature are semi-batch with limited modeling work. For this reason, a semi-batch system with combined cooling and reverse addition anti-solvent is modeled. To account for the volume change in a semi-batch system the number density functions are expressed as a redefined number density ($\tilde{n}(x,t) = V(t)n(x,t)$) (Nagy et al., 2008; Yang and Nagy, 2014). The modified PBM will be as follow:

$$\frac{\partial}{\partial t}\tilde{n}_{tc}(x,t) = -\frac{\partial}{\partial x}(G(x)\tilde{n}_{tc}(x,t)) + \delta(x)V(t)B \tag{8}$$

$$\frac{\partial}{\partial t}\tilde{n}_{cs}(x,t) = -\frac{\partial}{\partial x}(G(x)\tilde{n}_{cs}(x,t)) + \delta(x)V(t)B - \tilde{D}_{cs,agg}(x) \tag{9}$$

$$\frac{\partial}{\partial t}\tilde{n}_a(x,t) = -\frac{\partial}{\partial x}(G(x)\tilde{n}_a(x,t)) + \tilde{B}_{a,agg}(x) - \tilde{D}_{a,agg}(x) \tag{10}$$

$$\tilde{n}_{ca}(x,t) = \tilde{n}_{cs}(x,t) + \tilde{n}_a(x,t) \tag{11}$$

$$\tilde{D}_{cs,agg}(x) = \tilde{n}_{cs}(x,t)\int_0^\infty \beta(x,\lambda)\tilde{n}_{ca}(\lambda,t)d\lambda \tag{12}$$

$$\tilde{B}_{a,agg}(x) = \frac{x^2}{2}\int_0^x \frac{\beta((x^3-\lambda^3)^{1/3},\lambda)\tilde{n}_{ca}((x^3-\lambda^3),t)\tilde{n}_{ca}(\lambda,t)}{(x^3-\lambda^3)^{2/3}}d\lambda \tag{13}$$

$$\tilde{D}_{a,agg}(x) = \tilde{n}_a(x,t)\int_0^\infty \beta(x,\lambda)\tilde{n}_{ca}(\lambda,t)d\lambda \tag{14}$$

The above set of PBEs can be solved using the quadrature method of moments (QMOM) approximation for the redefined moments (Marchisio et al., 2003a, 2003b; Costa et al., 2007; Gimbun et al., 2009).

$$\tilde{\mu}_k = \int_0^\infty x^k\tilde{n}(x,t)dx \approx \sum_{i=1}^N w_i L_i^k \tag{15}$$

The quadrature approximation transformed set of PBEs can be written as:

$$\frac{d\tilde{\mu}_{tc,k}}{dt} = k\sum_{i=1}^N w_{tc,i}L_{tc,i}^{k-1}G(L_{tc,i}) + \delta(k)V(t)B \tag{16}$$

$$\frac{d\tilde{\mu}_{cs,k}}{dt} = k\sum_{i=1}^N w_{cs,i}L_{cs,i}^{k-1}G(L_{cs,i}) + \delta(k)V(t)B - \tilde{D}_{cs,agg}(w_{ca,i},L_{ca,i},w_{cs,i},L_{cs,i},k) \tag{17}$$

$$\frac{d\tilde{\mu}_{a,k}}{dt} = k\sum_{i=1}^N w_{a,i}L_{a,i}^{k-1}G(L_{a,i}) + \tilde{B}_{a,agg}(w_{ca,i},L_{ca,i},k) - \tilde{D}_{a,agg}(w_{ca,i},L_{ca,i},w_{a,i},L_{a,i},k) \tag{18}$$

$$\tilde{D}_{cs,agg}(w_{ca,i}, L_{ca,i}, w_{cs,i}, L_{cs,i}, k) = \sum_{i=1}^{N} w_{cs,i} L_{cs,i}^{k} \sum_{j=1}^{N} w_{ca,j} \beta(L_{cs,i}, L_{ca,j}) \quad (19)$$

$$\tilde{B}_{a,agg}(w_{ca,i}, L_{ca,i}, k) = \frac{1}{2} \sum_{i=1}^{N} w_{ca,i} \sum_{j=1}^{N} w_{ca,j} (L_{ca,i}^{3} + L_{ca,j}^{3})^{\frac{k}{3}} \beta(L_{ca,i}, L_{ca,j}) \quad (20)$$

$$\tilde{D}_{a,agg}(w_{ca,i}, L_{ca,i}, w_{a,i}, L_{a,i}, k) = \sum_{i=1}^{N} w_{a,i} L_{a,i} \sum_{j=1}^{N} w_{ca,j} \beta(L_{a,i}, L_{ca,j}) \quad (21)$$

$$\tilde{\mu}_{ca,k} = \tilde{\mu}_{cs,k} + \tilde{\mu}_{a,k} \quad (22)$$

The set of PBEs is solved with the product difference (PD) algorithm and the number of quadrature points used is $N = 3$ which solves for the weights (w_i) and abscissas (L_i). Details regarding the PD algorithm can be found in the literature (Gimbun et al., 2009; Gordon, 1968; Mcgraw, 1997). Matlab® *ode15s* is used to solve the set of ODEs.

4. Mass balance and kinetics

The mass balance equations used in the model for the semi-batch reverse addition anti-solvent crystallization of benzoic acid is derived as:

$$\frac{dV}{dt} = F_s \quad (23)$$

$$\frac{dC_S}{dt} = \frac{(C_{BA_0} - C_s)}{V} F_s - \frac{3\rho_c k_v G \tilde{\mu}_{tc,2}}{V} \quad (24)$$

$$\frac{dx_{SASR}}{dt} = \frac{F_s}{V_0} \quad (25)$$

$$M = \frac{\rho_c k_v \tilde{\mu}_{tc,3}}{V} \quad (26)$$

where V (mL) is the volume of mother liquor mixture, F_s (mL/min) is the flow rate of solution being added to the system, C_S (g mL^{-1}) is the solute (benzoic acid) concentration, C_{BA_0} (g mL^{-1}) is the solute concentration in the solution being fed, and x_{SASR} is the solution to anti-solvent ratio. In Eq. (24), ρ_c is the density of the crystal and k_v is the shape factor and are fixed at 1.316 (g mL^{-1}) and 0.524, respectively. For simplicity it is assumed that the solvent mixture density change is negligible. M (g mL^{-1}) represents the magma density of the slurry.

The nucleation and growth rate kinetics for traditional anti-solvent crystallization of benzoic acid were used for this study and taken from the literature (Ramisetty, 2013).

$$B = k_b(\mathcal{N})(1 + i * M)(S - 1)^{b(\mathcal{N})} \quad (27)$$

$$G = k_g(\mathcal{N})(S - 1)^{g(\mathcal{N})} \quad (28)$$

$$S = \frac{C_S}{C_{sat}} \quad (29)$$

Here the nucleation and growth kinetics depend on supersaturation, S, (which is generated by changes in the solution to anti-solvent ratio ($\mathcal{SASR}$) and temperature) and agitation rate, $\mathcal{N}$. The variable i is an empirical parameter that influences the extent to which a system is driven by primary or secondary nucleation. The i parameter is not given in the reference and hence will be used to do a parameter study on the effect of secondary nucleation on the results of the model formulation. The dependence of the rate constants on the agitation rate is shown in Table 2.

There are limited complete studies of the solubility of benzoic acid in ethanol-water mixtures for various concentrations and temperatures except for O'Grady's PhD thesis (O'Grady, 2007). In his study, O'Grady carried out various solubility experiments for benzoic acid at different temperatures and ethanol-water mixtures. The data from his work is taken and fit to a third order polynomial with respect to both temperature and solution to anti-solvent ration ($\mathcal{SASR}$) using the Matlab function *fit*. In Fig. 1, the y-axis (left) and z-axis (right) are read as the concentration of benzoic acid in ethanol expressed in g per mL.

The agglomeration kernel used for this study is a homogeneous kernel derived from the combination of the Brownian diffusion kernel and the Zauner and Jones (2000) and will be referred to as the Brownian + kernel. It is expressed as:

$$\beta(L_i, L_j) = a(b + c\varepsilon^{\frac{1}{2}} - d\varepsilon) S^{e} \frac{k_a (L_i + L_j)^2}{L_i L_j} \quad (30)$$

The first portion of the agglomeration kernel is composed of the parameters and process conditions defined by Zauner and Jones (2000) where a, b, c, d and e are constants, ε is the energy dissipation and S is the supersaturation. The energy dissipation is defined as follows:

$$\varepsilon = \frac{N_p d_s^5 \mathcal{N}^3}{V} \quad (31)$$

where N_p is the stirrer power number, d_s (m) is the diameter of the stirrer and $\mathcal{N}$ is the agitation rate over V, the volume of the slurry (Subero-Couroyer et al., 2006). The second part of the kernel is the Brownian portion that takes into account the surface area effect of the two particles partaking in the agglomeration and is divided by the product of the two particles which allows for a determination effect; as the particles get larger the effect of the Brownian portion of the kernel is reduced. This is appropriate as this model allows the agglomeration rate to decreases as the particles get larger, a common behavior seen in agglomeration in suspension techniques like spherical crystallization.

5. Agglomeration efficiency and porosity

As pointed out by Ochsenbein et al. (2015), one of the advantages of the coupled population balance model is that it allows for the development of physically relevant parameters. One parameter is the agglomeration efficiency. The coupled PBM framework allows for the population of all primary crystals, un-agglomerated crystals and agglomerates to be tracked, allowing for the determination of the efficiency of the agglomeration process with regards to the total number of crystals contained in the agglomerates.

Fig. 2 is a schematic representation of the three populations being tracked by the coupled PBM framework. As the figure depicts, the primary crystals population consist of each individual crystal outlined in green[1] within the green dashed box, the individual crystals left in suspension consist of those crystals circled in blue dotted lines and lastly the agglomerates consist of those particles circled in red solid lines. Expressed in terms of volume, Fig. 2 illustrates that the ratio of the volume of agglomerates to the volume of total primary crystals is a measure of the extent of agglomeration:

$$\%\ of\ agglomerated\ crystals = 100\left(\frac{V_a}{V_{tc}}\right) \quad (32)$$

[1] For interpretation of color in Fig. 2, the reader is referred to the web version of this article.

Table 2
Empirical kinetic constants retrieved from Ramisetty (2013).

$\mathcal{N}$ - agitation rate (rpm)	k_g (10^{-6})	g	k_b (10^7)	b
400	1.5	3.1	1.2	1.6
600	2.6	3.5	3.2	1.9
800	3.2	3.8	3.6	2.3

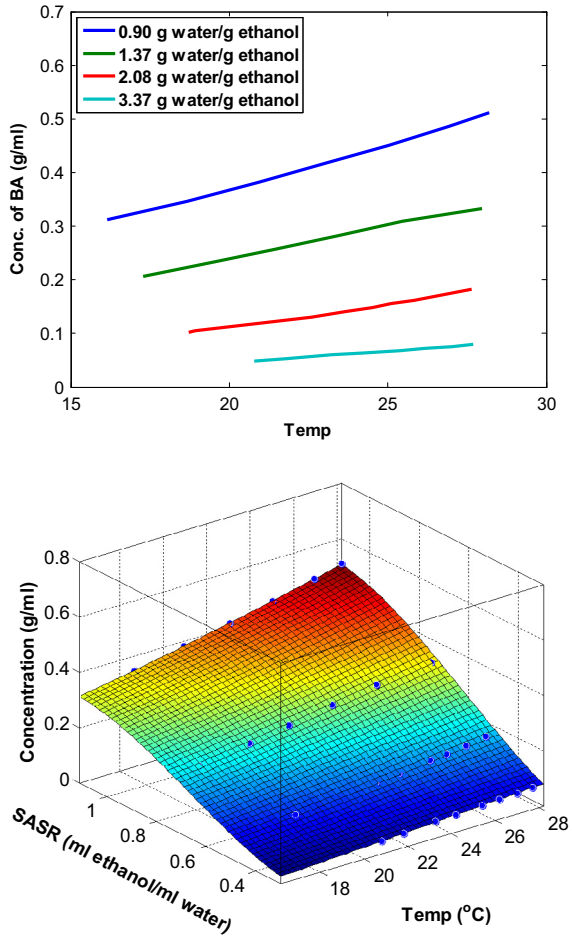

Fig. 1. (Left) Solubility data from O'Grady (2007) of benzoic acid in ethanol-water mixture with respect to temperature. (Right) Resulting solubility surface as a function of solution to anti-solvent ratio and temperature. The solution to anti-solvent ratios from O'Grady were expressed as volume ratios for the solubility surface.

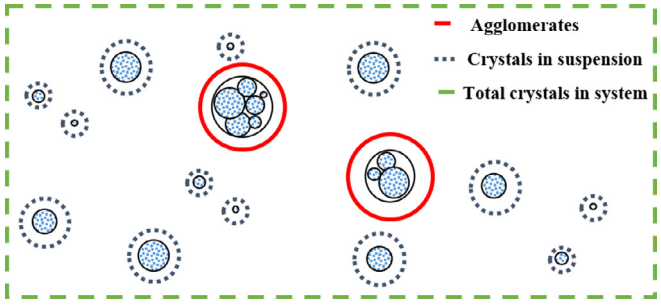

Fig. 2. Schematic of the different populations being tracked by the coupled PBM framework.

This definition can be very easily defined using the moments of the PBM ($\tilde{\mu}_{tc,k}, \tilde{\mu}_{cs,k}, \tilde{\mu}_{a,k}$). Specifically, the third moment of each PBE which is a volume based moment can be used to express the agglomeration efficiency as:

$$\mathcal{AE} = 100\left(\frac{\tilde{\mu}_{a,3}}{\tilde{\mu}_{tc,3}}\right) \tag{33}$$

Porosity is a property of interest in agglomeration and granulation due to the effects it can have on other properties like dissolution and compressibility. Many times a final desired porosity can determine the experimental conditions.

Fig. 3 illustrates how the porosity of an agglomerate decreases as subsequent agglomeration continues over time. Due to the one-dimensional PBE, reconstructing the size of the agglomerate from the characteristic length makes the assumption that the particle produced from an agglomeration event is a sphere. This assumption causes high porosity initially (see agglomerate on left in Fig. 3) which is similar to what occurs experimentally. As subsequent agglomeration continues the assumption of a sphere becomes more reasonable and the porosity decreases in the very same manner seen experimentally (left to right in Fig. 3). Expressed in terms of volume Fig. 3 states that volume of the pore (V_p) is equal to the volume of agglomerates minus the difference between the volume of primary crystals and volume of un-agglomerated crystals. The porosity determined by dividing this difference by the volume of agglomerates.

$$V_p = V_a - (V_{tc} - V_{cs}) \tag{34}$$

$$\varepsilon_p = 1 - \frac{(V_{tc} - V_{cs})}{V_a} \tag{35}$$

Similar to the agglomeration efficiency the porosity can be calculated with respect to the moments of the coupled PBM ($\tilde{\mu}_{tc,k}, \tilde{\mu}_{cs,k}, \tilde{\mu}_{a,k}$).

$$\mathcal{P} = 1 - \frac{\frac{\tilde{\mu}_{tc,3}}{\tilde{\mu}_{tc,0}} - \frac{\tilde{\mu}_{cs,3}}{\tilde{\mu}_{cs,0}}}{\tilde{\mu}_{a,3}/\tilde{\mu}_{a,0}} = 1 - \frac{\mathcal{V}_{tc,30} - \mathcal{V}_{cs,30}}{\mathcal{V}_{a,30}} \tag{36}$$

The aforementioned set of coupled population balance equations and defined parameters are to be used in an optimization framework where internal properties like crystal mean size and external properties like agglomerate mean size can be optimized for subject to constraints on agglomeration efficient and yield, and other quality attributes or process constraints.

6. Optimization framework

Three optimization scenarios were analyzed: (i) minimizing primary crystal size, (ii) maximizing primary crystal size, and (iii) attaining bioavailability and manufacturability targets. For simplicity the total particle mean size using the first and zeroth moment of the respective populations were used, $\mathcal{L}_{tc,10}$ and $\mathcal{L}_{a,10}$. The batch time is fixed at 300 min (~5 h) which is typical for agglomeration in suspension systems like benzoic acid spherical crystallization. The optimization variables are the dynamic operating profiles for temperature ($\mathcal{T}(\sqcup)$), agitation rate ($\mathcal{N}(\sqcup)$) and solution flow rate ($\mathcal{F}_f(\sqcup)$). The level of discretization for the optimization variables is 10. All the scenarios were subject to the same variable bounds and constraints. The bounds were chosen based on the range of the available solubility and kinetic data. The framework includes constraints on cooling/heating rate, ($\frac{\partial \mathcal{T}}{\partial \sqcup}$), solution addition ($\mathcal{SASR}$), agglomeration efficiency, ($\mathcal{AE}$), yield, ($\mathcal{C}_{final}$) and initial flow rate, ($\mathcal{F}_f(0)$). Due to the fact that a reverse addition anti-solvent crystallization system was chosen for this study the constraint on the initial flow rate assures that a certain crystal mass will be generated otherwise the optimizer may try to crystalize one large particle towards the end of the batch. The optimization problem for the first two scenarios can be written as:

$$\min_{\mathcal{T}(\sqcup),\mathcal{N}(\sqcup),\mathcal{F}_f(\sqcup)} -\mathcal{L}_{tc,10} \text{ or } \mathcal{L}_{tc,10} \tag{37}$$

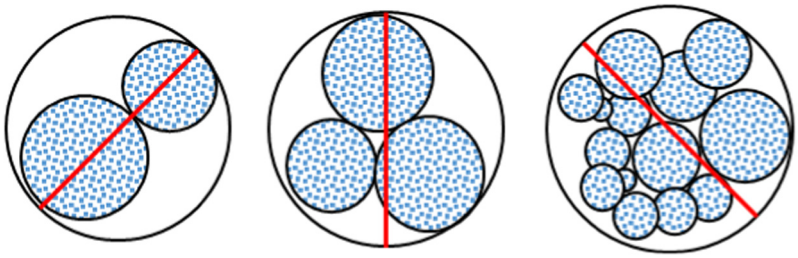

Fig. 3. Schematic of agglomerates with similar characteristic lengths but different internal properties (i.e. porosity).

s.t.

$$16 \leqslant \mathcal{T}(\sqcup) \leqslant 28\ ^{\circ}\mathrm{C} \tag{38}$$

$$400 \leqslant \mathcal{N}(\sqcup) \leqslant 800\ \mathrm{RPM} \tag{39}$$

$$0 \leqslant \mathcal{F}_{J}(\sqcup) \leqslant 2.5\ \mathrm{mL/min} \tag{40}$$

$$-0.4 \leqslant \frac{\partial \mathcal{T}}{\partial \sqcup} \leqslant 0.4\ ^{\circ}\mathrm{C/min} \tag{41}$$

$$0.25 \leqslant \mathcal{SASR} \leqslant 0.40 \tag{42}$$

$$\mathcal{AE} \geqslant 50\% \tag{43}$$

$$\mathcal{C}_{final} \leqslant 0.75\mathcal{C}_{max} \tag{44}$$

$$\mathcal{F}_{J}(0) \geqslant 1.0\ \mathrm{mL/min} \tag{45}$$

The new variable $\mathcal{C}_{final}$ is the final concentration of solute in solution while C_{max} is the maximum concentration if all the solution is added to the system and no crystallization occurred. As written the constraint requires a 25% yield. The optimization problem is solved using the "interior point" method of *fmincon* in Matlab. The objective function of the optimization problem for the last scenario can be written as:

$$\min_{\mathcal{T}(\sqcup),\mathcal{N}(\sqcup),\mathcal{F}_{J}(\sqcup)} \beth_1(B_T - \mathcal{L}_{tc,10})^2 + \beth_2(M_T - \mathcal{L}_{a,10})^2 \tag{46}$$

$\mathcal{B}_T$ and $\mathcal{M}_T$ represent bioavailability and manufacturability targets. For this scenario the optimization problem is a multi-objective framework with $\beth_1$ and $\beth_2$ being the weights for each objective. The weights in Eq. (46) are shown as a generalization for situations in which bioavailability or manufacturability is more heavily weighted than the other. In this work, $\beth_1$ and $\beth_2$ each have values of one. This scenario is restricted to the same constraints previously described.

7. Results and discussion

7.1. Minimizing primary particle mean size

The first scenario of interest is the minimization of the particle size. Minimization of primary crystal mean size is relevant in many industrial scenarios and helps with micromeritic properties in pharmaceutical applications like bioavailability and dissolution. This scenario will also serve to illustrate the capabilities of the coupled population balance model approach. The moments of this scenario illustrate the ability to keep track of all the populations in the PBE set. Fig. 4 shows the zeroth moment for the three populations. The zeroth moment is representative of the total particle count. In Fig. 4, the total particle count for the primary crystals in the system increases as solution is fed and the system becomes supersaturated. For this scenario, an inflection point occurs (at 105) indicating a significant increase in nucleation and a plateau is reached (at 220 min) indicative of zero supersaturation (zero nucleation).

Focusing on the zeroth moment of the un-agglomerated crystals and the agglomerates it can be seen that there is an initial increase in un-agglomerated crystals that correlates with that of the primary crystals when the system first nucleates. There is a delayed increase in the agglomerate counts since agglomeration cannot begin until there are crystals present. At 38 min, the un-agglomerated crystals count begins to spike but is then quickly reduced due to agglomeration. Since agglomerate formation can occur from crystal-crystal, crystal-agglomerate and agglomerate-agglomerate interactions, the zeroth moment of the agglomerates continues to decrease further; even though there is no longer nucleation (zeroth moment of primary crystals plateaus). The difference in magnitude of the primary crystals and un-agglomerated crystals in the beginning is also an indication of agglomeration.

Fig. 5 shows the third moment for the three populations. As the system begins to nucleate and grow the volume of the primary crystals increases steadily until the supersaturation is depleted. Comparing both Figs. 4 and 5 suggests that most of the particle volume is created at the onset with low total counts followed by secondary nucleation shown by the jump in the total counts but only a slight increase in total volume. The volume of un-agglomerated crystals is significantly smaller than the volume of primary crystals and agglomerates suggesting that most of the agglomeration happens at after the infliction (increase in nucleation) in primary crystals counts. The third moment of the three populations shows the same trend for all optimization scenarios investigated and hence will not be shown for other scenarios.

Comparing Figs. 4 and 5 can be misleading given that in Fig. 4 the total count of un-agglomerated crystals is increasing along with that of primary crystals, while in Fig. 5 the total volume of un-agglomerated crystals rapidly decreases and is significantly smaller than that of the primary crystals. This can be clarified by looking at the mean sizes of the three populations.

The mean size optimization profiles of the three populations for this scenario are shown in Fig. 6. The mean size is expressed as the

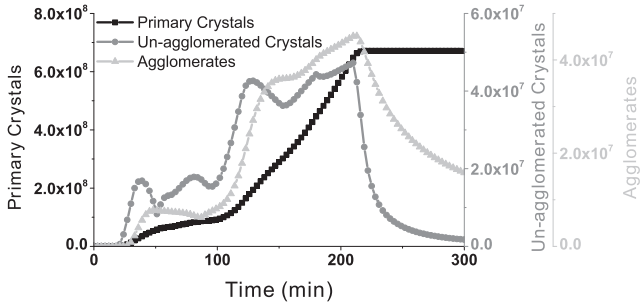

Fig. 4. The zeroth moment for each population in the PBE set for the minimization of $L_{tc,10}$.

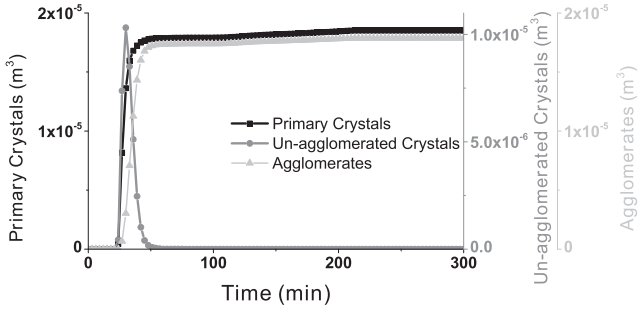

Fig. 5. The third moment for each population in the PBE set for the minimization of $L_{tc,10}$.

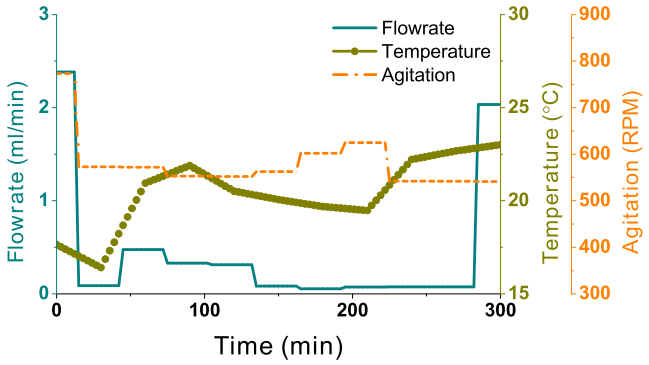

Fig. 7. Optimal flowrate, temperature and agitation rate profiles for the minimization of $L_{tc,10}$.

first moment divided by the zeroth, $L_{tc,10}$. The minimum primary particle size achievable in this scenario is 2.5 μm. While the crystals left in suspension have a mean size of 0.1 μm and the agglomerates are of a mean size of 28.8 μm. The small size of the un-agglomerated crystals again suggests that the increase seen in the total counts relates to secondary nucleation, which in turn corresponds to a small particle size and very small/negligible volume. The agglomerate mean size and the primary crystal mean size follow the trend observed from the zeroth moment. When the primary crystal mean size plateaus the agglomerate mean size increases otherwise they follow the same pattern as the primary crystal mean size increases the agglomerate mean size increases and vice versa.

Fig. 7 shows the optimal flowrate, temperature and agitation rate profiles for the minimization of the primary crystals mean size. Flowrate is initialized at its upper bound, the temperature profile starts near its lower bound and the agitation rate is initialized at its upper bound. High nucleation or crashing out is characteristic of reverse addition anti-solvent crystallization. As a result, the optimizer begins the process by nucleating from the addition of solution to the anti-solvent, at lower temperatures and high agitation rate to promote nucleation and generate small crystals. This period lasts the first 15 min and allows for the system to reach a supersaturated state quickly.

Immediately following the initial period, the flow rate of solution is decreased to its lower bound, the temperature begins to decrease further and the agitation rate is decreased to 600 RPM. These changes allow the system to decouple the effects of solution addition, temperature and agitation on nucleation. Whenever solution addition is increased, temperature is slightly increased and whenever solution addition is decreased, temperature is slightly decreased allowing for nucleation to be controlled by flowrate or temperature. This keeps the system supersaturated and in a nucleation phase, evident by the continued decrease in the primary crystals mean size, until the plateau in primary crystals is reached at 220 min. Nucleation is reduced in this period by an increase in temperature and solution addition. This period is continued until the end of the batch. This final addition of solution satisfies the solution to anti-solvent ratio constraint and decreases supersaturation. Fig. 8 shows the operating curve along the solubility surface for this scenario.

7.2. Maximizing primary particle mean size

Maximizing particle size also has industrial relevance in that some systems exhibit low downstream processing efficiency when the particle size is too small. For this scenario, Fig. 9 shows the primary crystal count very quickly reaching a plateau (100th min) indicative of the system avoiding secondary nucleation. A similar behavior in the zeroth moment of un-agglomerated crystals and agglomerate population is observed. The initial spike in the number of un-agglomerated crystals increases similarly to the primary crystals, however once the primary crystal counts plateau the counts of un-agglomerated crystals decreases sharply. This is followed by an increase and then a decrease in the agglomerate counts as the system transitions from crystal-crystal agglomeration to agglomerate-crystal and agglomerate-agglomerate agglomeration.

Fig. 10 shows the optimization results for the maximization of the primary particle size. The maximum achievable primary particle size is 41.8 μm. While the un-agglomerated crystals left in

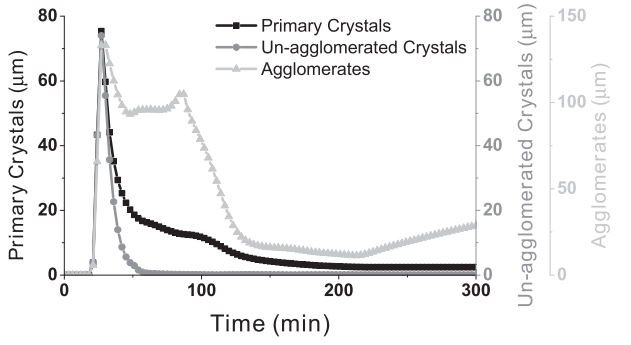

Fig. 6. Primary crystal mean size ($L_{tc,10}$), un-agglomerated crystals mean size ($L_{cs,10}$) and agglomerate mean size ($L_{a,10}$) for Scenario 1.

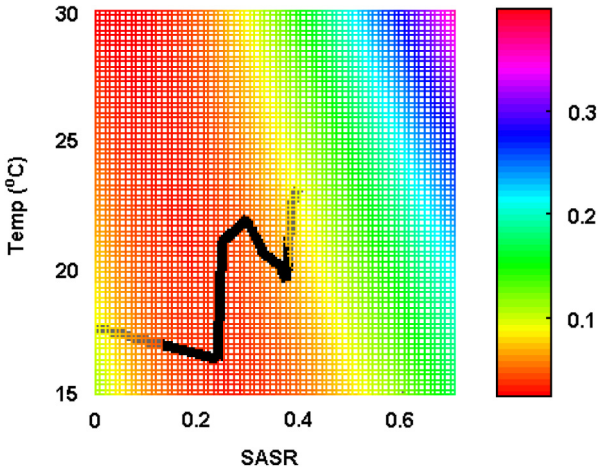

Fig. 8. Operating curve along the solubility surface for the minimization of primary crystal size.

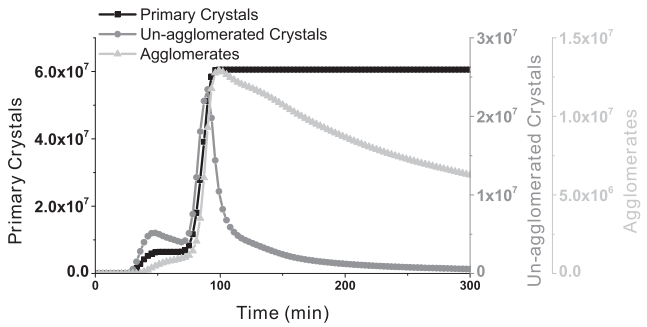

Fig. 9. The zeroth moment for each population in the PBE set for the maximization of $L_{tc,10}$.

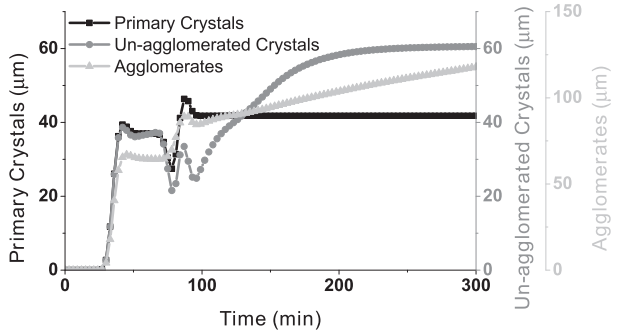

Fig. 10. Primary crystal mean size ($L_{tc,10}$), un-agglomerated crystals mean size ($L_{cs,10}$) and agglomerate mean size ($L_{a,10}$) for Scenario 2.

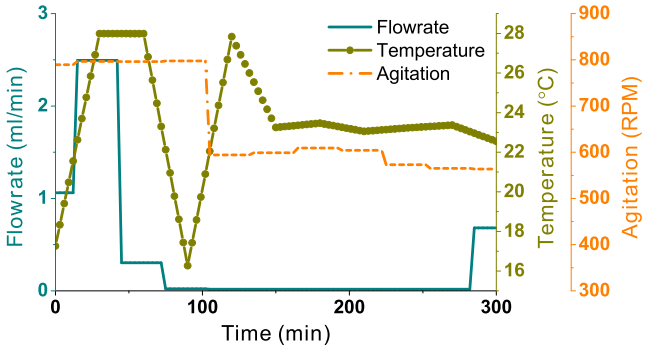

Fig. 11. Optimal flowrate, temperature and agitation rate profiles for the maximization of $L_{tc,10}$.

suspension have a mean size of 61.6 μm and the agglomerates are of a mean size of 117.8 μm. With regards to the growth of the primary crystals and agglomerates the trends are very similar to that of the first scenario. The mean size of the primary crystals remains constant after the 100th min which aligns with the plateau in primary crystals counts indicative of little supersaturation or growth beyond this point. As in the previous scenario, the agglomerate mean size increases when the primary crystal mean size is constant or when increasing. Interestingly, the un-agglomerated crystal mean size continues to increase even after the 100th min point. This is due to the agglomeration kernel used to describe the system. The Brownian + kernel favors the agglomeration of smaller particles. Hence, once the system plateaus with regards to counts and has depleted supersaturation; agglomeration will favor smaller particles, which is the reason for the increase in mean size of un-agglomerated crystals, due to the removal of fine crystals from this distribution. This is also the reason why the increase in the

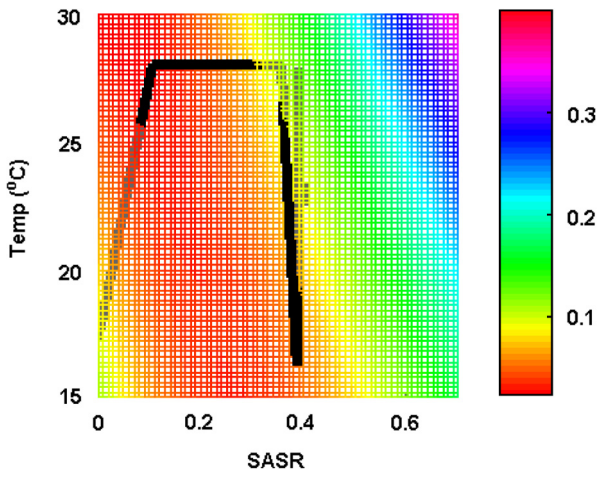

Fig. 12. Operating curve along the solubility surface for the maximization of primary crystal size.

mean size of un-agglomerated crystals increases with a higher order trend versus the agglomerate mean size which increases with a linear trend. Every small crystal that leaves the un-agglomerated crystals population increases the percentage of large crystals left behind while only marginally increasing the size of the agglomerate they attach to.

Fig. 11 shows the optimal process profiles for this scenario. The solution flow rate is initiated at 1.0 mL/min and quickly increased to the upper bound while the temperature is increased linearly to the upper bound (30 °C). As seen in Fig. 12 (solubility surface), the system is not supersaturated at the onset, and thus the delayed start in counts and mean size. As the solution flow rate is increased to 2.5 mL/min and the temperature is held constant, the system becomes supersaturated and crystals begin to nucleate and grow. The addition of solution is continued through the 75th minute until the system again becomes undersaturated. A steady decrease in temperature follows, bringing the system back to a supersaturated state. An increase in nucleation results as evident by the sharp increase in counts and subtle decrease in mean size. The process completes with another cycle of increasing temperature and decrease in agitation rate. This effectively serves to reduce the amount of supersaturation that is consumed due to nucleation and drives growth. This is evident by the increase in primary crystal mean size before the system plateaus and the temperature is brought to saturation.

7.3. Bioavailability and manufacturability targets

Optimizing for both bioavailability and manufacturability targets is the unique scenario that is made feasible by the proposed coupled population balance model framework. Prior to evaluating the attainability of bioavailability and manufacturability targets, the maximization of agglomerate particles is evaluated to understand the range and limitation to the maximum agglomerate size; although the optimal profiles are not shown here. The maximum attainable agglomerate size for the fixed batch time and operating conditions used here is 154.4 μm. The minimum and maximum size for the primary crystal were 2.5 and 41.8 μm, respectively. Given these results, the bioavailability target, B_T, for the mean size is set to 10 μm and the manufacturability target, M_T, is set to 50 μm.

Fig. 13 shows the results of the mean sizes for the bioavailability and manufacturability targets. Both the bioavailability and manufacturability target sizes were attained within 1 μm. $B_T = 10.1$ and $M_T = 49.9$ μm. The trends of mean size profiles

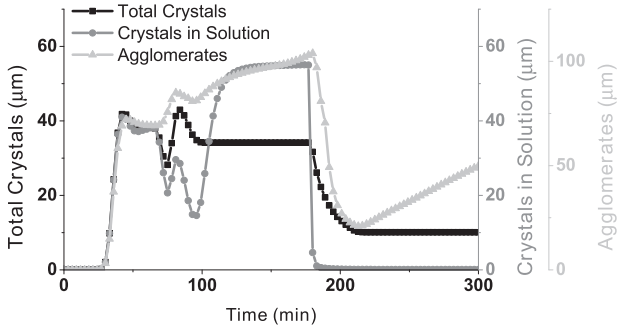

Fig. 13. Primary crystal mean size ($L_{tc,10}$), un-agglomerated crystals mean size ($L_{cs,10}$) and agglomerate mean size ($L_{a,10}$) for Scenario 3.

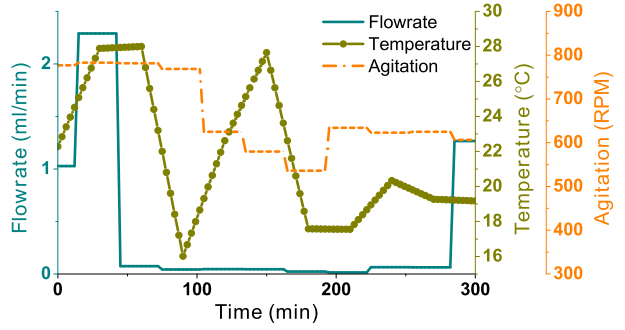

Fig. 14. Optimal flowrate, temperature and agitation rate profiles for the bioavailability and manufacturability target.

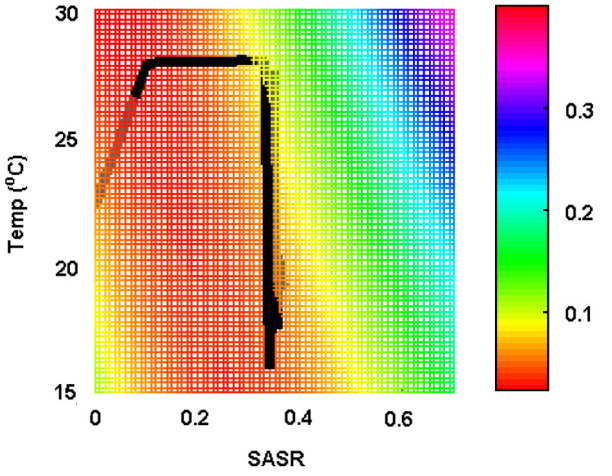

Fig. 15. Operating curve along the solubility surface for the bioavailability and manufacturability targets.

described for the previous scenario is similar in this scenario. When the primary crystals mean size is increasing or constant the agglomerate mean size increases. While the primary crystal mean size is constant the un-agglomerated crystal mean size increases because agglomeration favors smaller particles due to the agglomeration kernel used in this case. All the mean sizes decrease when nucleation occurs due to the increase in smaller counts for all populations.

Fig. 14 shows the optimal process profiles for the solution flow rate, temperature and agitation and Fig. 15 shows the operating line along the solubility surface. Analyzing these figures together, it is obvious that the optimal profile is a combination or interpolation of the previous two scenarios. One apparent difference is the number of temperature cycles observed in this scenario driven by the need to balance both nucleation and growth of the primary crystals so to attain both targets. From a solution flow rate perspective, the system is initiated and carried in the same manner as the previous scenario of maximizing primary particle size. The solution flow rate is initiated at 1.0 mL/min and then increased to the upper bound while the temperature is increased linearly to the upper bound (30 °C). As in the previous scenario, the system is undersaturated until the solution flow rate is increased (Fig. 15). A temperature cycling phase then commences at a very low solution addition. This temperature cycles and low solution addition balance nucleation and growth allowing for both the bioavailability and manufacturability targets to be reached. The agitation rate follows the same trend as both previous scenarios.

The agitation profile is fairly similar for all three scenarios indicating that agitation rate is impacting the nucleation and growth kinetics more than the agglomeration kinetics. Overall the trend in agglomerate size with respect to changes in agitation rate did not match those reported in the literature (Kawashima, 1984, 1995; Katta and Rasmuson, 2008). This is most likely due to the set of nucleation and growth kinetic models used as both have an agitation rate dependence. The influence temperature profiles also had an impact on this results since most spherical agglomeration experiments had previously been conducted at constant temperature.

Table 3 summarizes the optimization results. All scenarios met the agglomeration efficiency (larger than 50%), yield (25% or greater) and SASR constraints (between 0.25 and 0.40). The bioavailability and manufacturing target scenario required the lowest amount of solution to the system but produced the highest yield. This is most likely due to the greater number of temperature cycles. The scenario to minimize primary crystal mean size had lowest yield most likely due to prevention of growth in the system. This scenario also had the highest agglomeration efficiency which is also related to the high amount of nucleation in this scenario and the fact that agglomeration favors smaller particles.

Table 3
Summary of optimization results with constraint values.

Parameters	*Min* $L_{tc,10}$	*Max* $L_{tc,10}$	B_T/M_T
$L_{tc,10}$ (μm)	2.5	41.8	10.1
$L_{a,10}$ (μm)	28.8	117.8	49.9
AE (%)	96.5	77.5	75.6
Yield	0.25	0.31	0.41
SASR	0.39	0.40	0.37

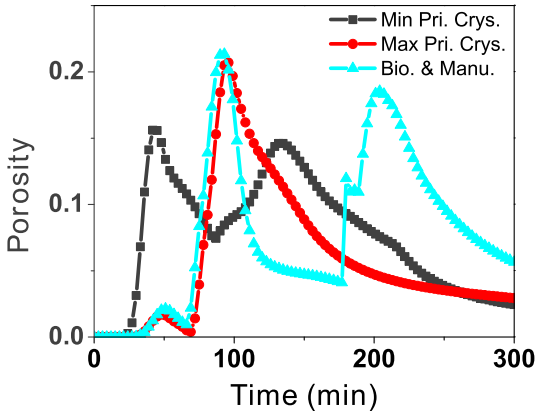

Fig. 16. Porosity profiles for all three optimization scenarios.

Table 4
Comparison of optimization results with different ***i*** values.

Empirical parameter	*Min* $L_{tc,10}$ $L_{tc,10}/L_{a,10}$ (μm)	*Max* $L_{tc,10}$ $L_{tc,10}/L_{a,10}$ (μm)
i = 1	2.5/28.8	41.8/117.8
i = 0.01	19.8/145.8	89.6/156.1

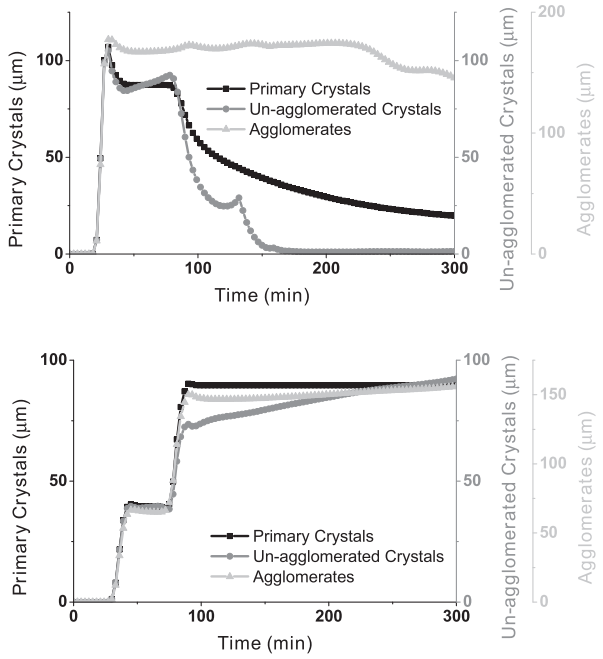

Fig. 17. Primary crystal mean size ($L_{tc,10}$), un-agglomerated crystal mean size ($L_{cs,10}$) and agglomerate mean size ($L_{a,10}$) when i = 0.01 for both minimization (left) and maximization (right) of primary crystal size.

Fig. 16 shows the porosity profiles from the optimization scenarios. As detailed in the model development section, this approach to estimating porosity is unique and derived from the moments of the distributions. The benefits of calculating porosity in simulations is the ability to design process around the ideal porosity for specific dissolution and compression properties. The porosity is not included in the optimization studies as it would require an appropriate scaling parameter to make physical sense. The porosity for the different scenarios show similar final values with different profiles. The porosity profile for the maximization of primary crystal size increases initially and then decreases as the system continues to agglomerate without supersaturation or nucleation (Figs. 9 and 10). The profiles for the minimization of primary crystal size and target bioavailability and manufacturability both follow similar cycles of increasing and decreasing porosity, which correlates well with the temperature and nucleation cycles seen in optimal profiles and total counts.

7.4. Effects of secondary nucleation

The parameters used for the presented results were taken from literature values. However, the empirical parameter ***i*** found in the nucleation rate expression is not found in the literature and was not fit to experimental data prior to this study. A study to understand the effects of this parameter on the simulation and optimization results was conducted. Table 4 shows the differences in the results for minimization and maximization of primary crystal for ***i*** equal to 1 and 0.01.

The results from shown in Table 4 show that a lower ***i*** value results in a significantly larger achievable minimum and maximum primary crystal mean size. Modulating ***i*** varies the extent of secondary nucleation in the system. A lower ***i*** value decreases the extent of secondary nucleation which in return allows more supersaturation to be consumed by growth.

Fig. 17 shows the mean size profiles for both the minimization and maximization of primary crystal size. The mean size profiles show a significant difference from that of the system with a higher value for ***i***. Most notably, changes in the mean size for the agglomerate follow more closely the changes in mean size of the primary crystals. The agglomerate mean size stays relatively constant, increases and decreases with the same trend as primary crystal mean size. This shows the impact that secondary nucleation can have on the final agglomerated size. The trends observed with lower values for ***i*** are more reasonable when compared to the experiments in the literature (Rasmuson and Thati, 2011; Thati and Rasmuson, 2012), but will need to be fit to experimental data to attain a system specific value.

8. Conclusions

In this work, a coupled population balance model with nucleation, growth and agglomeration was developed. Three populations of interest are tracked: primary crystals, un-agglomerated crystals and agglomerate populations. Tracking these populations separately gives access to otherwise unattainable information in traditional population balance models. This allows for optimization frameworks and process design efforts tailored to the property specifications for each population.

An optimization framework has been developed to achieve optimal flowrate, temperature and agitation rate profiles for a reverse addition, anti-solvent crystallization system of benzoic acid with agglomeration. The results of this work show that operating parameters can be optimized to achieve the desired primary and/or agglomerate properties. The framework allows for bioavailability (primary crystal size) and manufacturability (agglomerate particle size) optimization. Moving forward this model formulation will allow for the development of better, more relevant kinetic and agglomeration parameters. Given that each population is tracked separately, kinetic parameters can be fit separately without having to lump all the kinetics into one population; thereby increasing accuracy of the parameter fit. Agglomeration kernel identification would greatly improve with this model formulation, and can begin the shift from purely empirical kernels to combination kernels that relate the physical mechanisms and operating conditions more accurately. Moving forward the proposed model formulation will be fit to data from various agglomeration in suspension systems to assess its capability to predict product properties.

Acknowledgements

Eli Lilly & Co. for their advice and funding support through the Lilly Research Award Program. Special thanks Omar José Guerra Fernández and Francesco Rossi from Dr. Reklaitis's research group at Purdue University.

References

Amaro-González, D., Biscans, B., 2002. Spherical agglomeration during crystallization of an active pharmaceutical ingredient. Powder Technol. 128, 188–194. http://dx.doi.org/10.1016/S0032-5910(02)00196-1.

Bemer, G.G., 1979. Agglomeration in Suspension: A Study of Mechanisms and Kinetics. Technische Hogeschool Delft, The Netherlands.

Blandin, A.F., Mangin, D., Rivoire, A., Klein, J.P., Bossoutrot, J.M., 2003. Agglomeration in suspension of salicylic acid fine particles: influence of some process parameters on kinetics and agglomerate final size. Powder Technol. 130, 316–323.

Blandin, A.F., Mangin, D., Subero-Couroyer, C., Rivoire, A., Klein, J.P., Bossoutrot, J.M., 2005. Modelling of agglomeration in suspension: application to salicylic acid microparticles. Powder Technol. 156 (1), 19–33. http://dx.doi.org/10.1016/j.powtec.2005.05.049.

Brunsteiner, M., Jones, A.G., Pratola, F., Price, S.L., Simons, S.J.R., 2005. Toward a molecular understanding of crystal agglomeration. Cryst. Growth Des. 5 (1), 3–16. http://dx.doi.org/10.1021/cg049837m.

Costa, C.B.B., Maciel, M.R.W., Filho, R.M., 2007. Considerations on the crystallization modeling: population balance solution. Comput. Chem. Eng. 31 (3), 206–218. http://dx.doi.org/10.1016/j.compchemeng.2006.06.005.

Coulaloglou, C.A., Tavlarides, L.L., 1977. Description of interaction processes in agitated liquid-liquid dispersions. Chem. Eng. Sc. 32 (11), 1289–1297. http://dx.doi.org/10.1016/0009-2509(77)85023-9.

David, R., Marchal, P., Klein, J.P., Klein, J.V., 1990. Crystallization and precipitation engineering III. A discrete formulation of the agglomeration rate of crystals in a crystallization process. Chem. Eng. Sci. 46 (1), 205–213. http://dx.doi.org/10.1016/0009-2509(91)80130-Q.

David, R., Paulaime, A.-M., Espitalier, F., Rouleau, L., 2003. Modelling of multiple-mechanism agglomeration in a crystallization process. Powder Technol. 130 (1–3), 338–344. http://dx.doi.org/10.1016/S0032-5910(02)00213-9.

Gimbun, J., Nagy, Z.K., Rielly, C.D., 2009. Simultaneous quadrature method of moments for the solution of population balance equations, using a differential algebraic equation framework. Ind. Eng. Chem. Res. 48 (16), 7798–7812. http://dx.doi.org/10.1021/ie900548s.

Gordon, R.G., 1968. Error bounds in equilibrium statistical mechanics. J. Math. Phys. 9 (5), 655. http://dx.doi.org/10.1063/1.1664624.

Iveson, S.M., 2002. Limitations of one-dimensional population balance models of wet granulation processes. Powder Technol. 124 (3), 219–229. http://dx.doi.org/10.1016/S0032-5910(02)00026-8.

Katta, J., Rasmuson, A.C., 2008. Spherical crystallization of benzoic acid. Int. J. Pharm. 348, 61–69.

Kawashima, Y., 1984. Development of spherical crystallization technique and its application to pharmaceutical systems. Arch. Pharm. Res. 7 (2), 145–151.

Kawashima, Y., 1995. Parameters determining the agglomeration behaviour and the micromeritic properties of spherically agglomerated crystals prepared by the spherical crystallization technique with miscible solvent systems. Int. J. Pharm. 119, 139–147.

Kawashima, Y., Capes, C., 1974. An experimental study of the kinetics of spherical agglomeration in a stirred vessel. Powder Technol. 10, 85–92.

Kawashima, Y., Kurachi, Y., Takenaka, H., 1982a. Preparation of spherical wax matrices of sulfamethoxazole by wet spherical agglomeration technique using a CMSMPR agglomerator. Powder Technol. 32, 155–161.

Kawashima, Y., Okumura, M., Takenaka, H., 1982b. Spherical crystallization: direct spherical agglomeration of salicylic acid crystals during crystallization. Science 20–21.

Kawashima, Y., Imai, M., Takeuchi, H., Yamamoto, H., Kamiya, K., Hino, T., 2003. Improved flowability and compactibility of spherically agglomerated crystals of ascorbic acid for direct tableting designed by spherical crystallization process. Powder Technol. 130, 283–289.

Kuboi, R., Nienow, A.W., Conti, R., 1984. Mechanical attrition of crystals in stirred vessels. Ind. Crystall. 84, 211–216.

Kumar, S., Ramkrishna, D., 1997. On the solution of population balance equations by discretization—III. Nucleation, growth and aggregation of particles. Chem. Eng. Sci. 52 (24), 4659–4679. http://dx.doi.org/10.1016/S0009-2509(97)00307-2.

Liu, L.X., Litster, J.D., 2002. Population balance modelling of granulation with a physically based coalescence kernel. Chem. Eng. Sci. 57 (12), 2183–2191. http://dx.doi.org/10.1016/S0009-2509(02)00110-0.

Madec, L., Falk, L., Plasari, E., 2003. Modelling of the agglomeration in suspension process with multidimensional kernels. Powder Technol. 130, 147–153. http://dx.doi.org/10.1016/S0032-5910(02)00258-9.

Marchal, P., David, R., Klein, J.P., Villermaux, J., 1988. Crystallization and precipitation engineering—I. An efficient method for solving population balance in crystallization with agglomeration. Chem. Eng. Sci. 43, 59–67. http://dx.doi.org/10.1016/0009-2509(88)87126-4.

Marchisio, D.L., Pikturna, J.T., Fox, R.O., Vigil, R.D., Barresi, A.A., 2003a. Quadrature method of moments for population-balance equations. AIChE J. 49 (5), 1266–1276. http://dx.doi.org/10.1002/aic.690490517.

Marchisio, D.L., Vigil, R.D., Fox, R.O., 2003b. Quadrature method of moments for aggregation–breakage processes. J. Colloid Interface Sci. 258 (2), 322–334. http://dx.doi.org/10.1016/S0021-9797(02)00054-1.

Mcgraw, R., 1997. Description of aerosol dynamics by the quadrature method of moments. Aerosol Sci. Technol. 27 <http://www.tandfonline.com/doi/pdf/10.1080/02786829708965471>.

Nagy, Z.K., Fujiwara, M., Braatz, R.D., 2008. Modelling and control of combined cooling and antisolvent crystallization processes. J. Process Control 18 (9), 856–864. http://dx.doi.org/10.1016/j.jprocont.2008.06.002.

Nagy, Z.K., Fevotte, G., Kramer, H., Simon, L.L., 2013. Recent advances in the monitoring, modelling and control of crystallization systems. Chem. Eng. Res. Des. 91 (10), 1903–1922.

O'Grady, D., 2007. Multiscale Characterization of Anti-Solvent Crystallization PhD thesis. University College Dublin, Ireland.

Ochsenbein, D.R., Vetter, T., Morari, M., Mazzotti, M., 2015. Agglomeration of needle-like crystals in suspension: II. modeling. Cryst. Growth Des. 15 (9), 4296–4310. http://dx.doi.org/10.1021/acs.cgd.5b00604.

Peña, R., Nagy, Z.K., 2015. Process intensification through continuous spherical crystallization using a two-stage mixed suspension mixed product removal (MSMPR) system. Cryst. Growth Des. 15 (9), 4225–4236.

Petela, R., 1991. Prediction of the product size in the agglomeration of coal particles in a water-oil emulsion. Fuel 70, 509–517.

Prince, M.J., Blanch, H.W., 1990. Bubble coalescence and break-up in air-sparged bubble columns. AIChE J. 36 (10), 1485–1499. http://dx.doi.org/10.1002/aic.690361004.

Ramisetty, K., 2013. Ultrasound-assisted antisolvent crystallization of benzoic acid: effect of process variables supported by theoretical simulations. Ind. Eng. Chem. Res. <http://pubsacs.org/doi/abs/10.1021/ie402203k>.

Ramkrishna, D., 2000. Population Balances Theory and Applications to Particulate Systems in Engineering. Academic Press, San Diego, CA.

Randolph, A., Larson, M., 1971. Theory of Particulate Processes; Analysis and Techniques of Continuous Crystallization. Academic Press, New York.

Rasmuson, A.C., Thati, J., 2011. On the mechanisms of formation of spherical agglomerates. Eur. J. Pharm. Sci. 42, 365–379.

Seyssiecq, I., Veesler, S., Mangin, D., Klein, J.P., Boistelle, R., 2000. Modelling gibbsite agglomeration in a constant supersaturation crystallizer. Chem. Eng. Sci. 55, 5565–5578. http://dx.doi.org/10.1016/S0009-2509(00)00185-8.

Smoluchowski, M.V., 1917. Z. Phys. Chem. 19, 129–168.

Subero-Couroyer, C., Mangin, D., Rivoire, A., Blandin, A.F., Klein, J.P., 2006. Agglomeration in suspension of salicylic acid fine particles: analysis of the wetting period and effect of the binder injection mode on the final agglomerate size. Powder Technol. 161, 98–109. http://dx.doi.org/10.1016/j.powtec.2005.08.014.

Thati, J., Rasmuson, A.C., 2012. Particle engineering of benzoic acid by spherical agglomeration. Eur. J. Pharm. Sci. 45, 657–667.

Yang, Y., Nagy, Z.K., 2014. Model-based systematic design and analysis approach for unseeded combined cooling and antisolvent crystallization (CCAC) systems. Cryst. Growth Des. 14 (2), 687–698. http://dx.doi.org/10.1021/cg401562t.

Zauner, R., Jones, A.G., 2000. Determination of nucleation, growth, agglomeration and disruption kinetics from experimental precipitation data: the calcium oxalate system. Chem. Eng. Sci. 55 (19), 4219–4232.